




Article

Non-Invasive Evaluation of Polymeric Protective Coatings for Metal Surfaces of Cultural Heritage Objects: Comparison of Optical and Electromagnetic Methods

Diego Quintero Balbas ¹, Alice Dal Fovo ¹, Daniela Porcu ^{1,2,3}, Antonina Chaban ¹, Simone Porcinai ⁴, Raffaella Fontana ¹ and Jana Striova ^{1,*}

¹ National Research Council—National Institute of Optics (CNR-INO), Largo E. Fermi 6, 50125 Florence, Italy; diegoivan.quinterobalbas@ino.cnr.it (D.Q.B.); alice.dalfovo@ino.cnr.it (A.D.F.); daniela.porcu@unifi.it (D.P.); antonina.chaban@ino.cnr.it (A.C.); raffaella.fontana@ino.cnr.it (R.F.)

² Department of Chemistry “Ugo Schiff”, University of Florence, Via della Lastruccia 3-13, 50019 Sesto Fiorentino, Italy

³ Center for Colloid and Surface Science, University of Florence, Via della Lastruccia 3, 50019 Sesto Fiorentino, Italy

⁴ Laboratorio Scientifico, Opificio delle Pietre Dure–MiC, Viale F. Strozzi, 1, 50129 Firenze, Italy; simone.porcinai@beniculturali.it

* Correspondence: jana.striova@cnr.it

Featured Application: Non-invasive measurement of protective coatings applied to metallic surfaces for monitoring their efficacy in the conservation of cultural heritage.



Citation: Quintero Balbas, D.; Dal Fovo, A.; Porcu, D.; Chaban, A.; Porcinai, S.; Fontana, R.; Striova, J. Non-Invasive Evaluation of Polymeric Protective Coatings for Metal Surfaces of Cultural Heritage Objects: Comparison of Optical and Electromagnetic Methods. *Appl. Sci.* **2022**, *12*, 7532. <https://doi.org/10.3390/app12157532>

Academic Editor: Guijun Bi

Received: 23 June 2022

Accepted: 25 July 2022

Published: 27 July 2022

Publisher’s Note: MDPI stays neutral with regard to jurisdictional claims in published maps and institutional affiliations.



Copyright: © 2022 by the authors. Licensee MDPI, Basel, Switzerland. This article is an open access article distributed under the terms and conditions of the Creative Commons Attribution (CC BY) license (<https://creativecommons.org/licenses/by/4.0/>).

Abstract: The application of protective coatings is an effective preventive strategy to avoid metal corrosion. Constant monitoring of the coating’s quality is fundamental for the successful preservation of the metallic objects by reducing their interaction with corroding agents. Their evaluation over time helps to identify failure at early stages and promote their removal and substitution. Several methods have been employed for coating evaluation (i.e., chemical analysis, thickness and homogeneity investigation). In this paper, we compare three methods—Optical Coherence Tomography (OCT), Confocal Raman Microspectroscopy (CRM), and Eddy Currents (ECs)—to evaluate thickness values and coating integrity. The results from the two optical techniques (CRM and OCT) agree, being able to detect the inhomogeneity of the layer on a micron scale but requiring correction to account for the refraction phenomenon. The Eddy Current is a fast and efficient method for thickness estimation, providing data with millimetric lateral resolution.

Keywords: protective coatings; cultural heritage; OCT; Confocal Raman; Eddy Current; metallic surfaces

1. Introduction

Metal corrosion has an economic and safety impact in several fields, such as automotive and oil industries and civil engineering [1]. In cultural heritage artifacts, corrosion products developed over centuries represent part of their history; consequently, they are generally preserved or partially removed. However, active corrosion phenomena can damage the objects, particularly those made of iron and copper alloys [2–4]. In this scenario, conservators implement protection and inhibition treatments and strategies to avoid further active degradation. For centuries, the application of protective coatings (e.g., resins, natural and synthetic waxes, cellulose derivatives, or acrylic-based polymers) has been an effective method for this purpose [2,3]. While not completely isolating the metallic surface [5], they can slow down the corrosion phenomena by reducing access to oxidizing agents and other pollutants [6]. A limited number of materials are suitable for application on metal-based cultural heritage objects because of the reversibility and stability characteristics required by conservation standards [2,4,7].

The effectiveness of protective coatings must be checked after their application and by constant monitoring throughout their lifespan, which can prompt coating substitution by conservators when signs of failure are detected (Figure 1) [8,9]. Several coating features may be monitored, including (a) chemical composition, (b) the application of the coating (particularly the thickness and homogeneity of the layer), (c) coating texture (i.e., porosity, roughness), and (d) electrochemical properties [8]. Different techniques have been tested to find suitable, easy, fast and non-destructive tools for conservators to constantly monitor the condition of a protective coating. This should preferably be performed at macro scale by mapping or by testing different areas of the object to determine the adequate time to remove and substitute the layers.

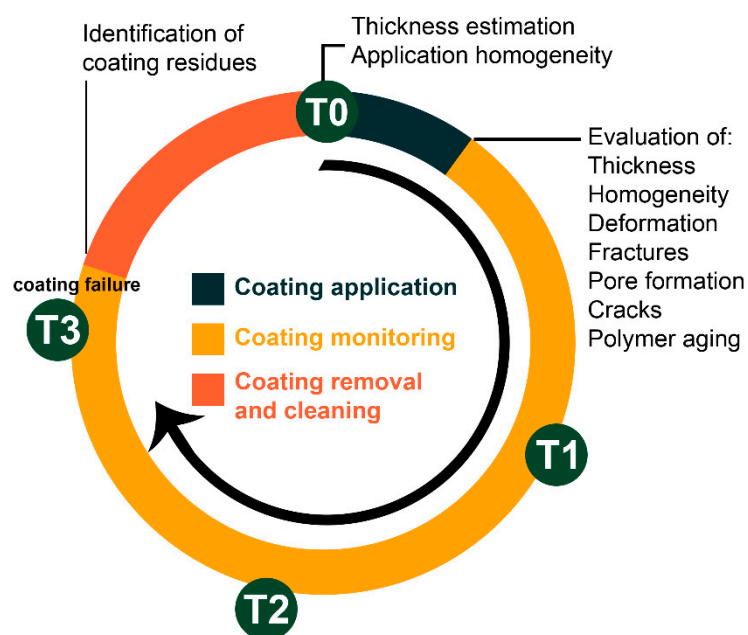


Figure 1. Schematic representation of a cycle of evaluation and monitoring of a protective coating applied to a metallic surface in cultural heritage. Labels T0–T3 represent the different analytical campaigns required to monitor the coating performance through time.

Evaluation of the electrochemical properties, which generally requires direct contact between the probe and the object surface, is a relatively common approach in the metal conservation field because of its ease of use and portability. Eddy Currents (ECs) [10] allow for thickness estimation through sample conductivity (σ) measurement. This is performed by detecting the impedance variation induced by the secondary magnetic field produced by the sample as a result of the Eddy Currents [11,12]. Recently, innovative EC set-ups have been developed with more accurate thickness measurements, sometimes achieved through a contactless modality [13]. Electrochemical Impedance Spectroscopy (EIS), on the other hand, aids in inspecting protective coatings applied to different metallic objects by evaluating their barrier properties [2,4]. Despite the valuable complementary information provided, it might operate with limited lateral resolution, long acquisition times, and considerable uncertainty regarding the quantification of coating thickness [14].

In the last few decades, alternative systems to evaluate and monitor protective coatings have been tested. X-ray fluorescence spectroscopy (XRF) has been applied to measure and map the thickness of coating layers on silver artifacts [15,16]. The most recent advances in molecular spectroscopy, such as reflectance Fourier-transform infrared (rFTIR) and Near-infrared (NIR), have shown promising results for studying the chemical composition and evaluating the homogeneity of protectives on bronze surfaces [17]. Other optical methods, such as Fiber Optic Reflectance Spectroscopy (FORS) [18], UV-induced visible fluorescence imaging [19], Fluorescence Lifetime Imaging (FLI) [20], ellipsometry [21] and

Optical Coherence Tomography (OCT) [14,22], are suitable tools for measuring protective coatings, yet their employment in metal conservation is still limited. Confocal Raman Microspectroscopy (CRM) is another non-destructive tool suitable for coating evaluation (i.e., thickness, homogeneity and distribution of chemical species) [23,24]; however, it is refraction-limited due to spherical aberration and laser refraction, particularly when testing with dry objectives, producing depth resolution broadening [23–25]. This inconvenience can be overcome by employing oil-immersion objectives or mathematical corrections [23]. CRM spatial resolution can be improved by coupling it to an Atomic Force Microscope (AFM) [26].

In this work, we compare the potential of three techniques: two portable techniques—Eddy Current (EC), widely used by conservators, and Optical Coherence Tomography (OCT)—and benchtop Confocal Raman Microspectroscopy (CRM), to evaluate film thickness of three of the most commonly used polymers in metal preservation—two acrylic copolymers (Paraloid[®] B-72 and Paraloid[®] B-44) and one cellulose nitrate lacquer (Zapon[®]). We aim to identify the advantages and disadvantages of each technique along with their complementarity, as well as the critical analytical points that should be considered. Our goal is to offer a methodological comparison that would allow professionals in charge of the preservation of metallic cultural heritage to make informed decisions. The data evidenced each technique's advantages (e.g., portability, precision, and ease of use) and drawbacks (e.g., optical aberrations or poor lateral resolution), providing an overview of critical characteristics. These data are presented with the aim of guiding the formulation of analytical strategies.

2. Materials and Methods

2.1. Sample Preparation

We evaluated two polymer classes, including two acrylic and one cellulose nitrate lacquer. Paraloid[®] B-72 (PB-72) (CTS, Vicenza, Italy) is a copolymer of methyl acrylate and ethyl methacrylate widely used in conservation as an adhesive, consolidant, and protective layer [27–31]. Paraloid[®] B-44 (PB-44) (CTS, Italy) is the commercial name for methyl methacrylate and ethyl acrylate copolymer, part of the Incralac[®] coating formulation [29]. Having a higher glass transition temperature (T_g) compared to PB-72, PB-44 is preferable for application in places where the temperature is higher than 40 °C [30].

Zapon[®] (Lechler, Italy), on the other hand, is a lacquer containing cellulose nitrate polymer soluble in different solvents (e.g., amyl acetate, butyl acetate, and propyl acetate or ethanol, ethyl acetate, and ethyl glycol) that conservators employ as a varnish, adhesive, and consolidant [32,33].

We studied nine transparent polymer disks (Table 1) of 13 mm (± 1 mm) in diameter obtained by depositing 35 μ L of the polymer, dissolved in butyl acetate at different concentrations, over a KBr pellet. After one week of curing, the KBr substrate was dissolved in distilled water, and the polymer disks were left to dry for 24 h under laboratory conditions.

Table 1. Summary of the samples studied in this work.

Polymer	Chemical Composition	Refractive Index	T_g (° C)	Sample Code	Concentration in Butyl Acetate (W %)
Paraloid [®] B-72	methyl acrylate/ethyl methacrylate copolymer	1.49 [34]	40	PB-72 ₃₀	30
				PB-72 ₂₅	25
				PB-72 ₁₀	10
Paraloid [®] B-44	methyl methacrylate/ethyl acrylate copolymer	1.48 [35]	60	PB-44 ₂₅	25
				PB-44 ₁₀	10
				PB-44 ₅	5
Zapon [®]	cellulose nitrate (Lacquer 30% v)	1.54 [28]	100	Zapon ₇₀	70 (poly. conc. = ~21% v)
				Zapon ₄₀	40 (poly. conc. = ~12% v)
				Zapon ₂₀	20 (poly. conc. = ~6% v)

2.2. Spectral-Domain Optical Coherence Tomography (SD-OCT)

For each disk, we performed 12 cross-sectional analyses (B-scans), spaced 1 mm apart, with a commercial SD-OCT device (Thorlabs Telesto-II). The device source is a superluminescent diode with a central wavelength of 1300 nm and a bandwidth of about 100 nm. The axial resolution in the air is 5.5 μm , while the lateral resolution is 13 μm . The detector consists of a spectrograph made of a diffraction grating and a fast camera. The system is controlled via 64-bit software preinstalled on a high-performance computer. The 3D scanning path probe with an integrated video camera performs high-speed imaging (76 kHz) for rapid volume acquisition and live display. The XZ acquisition field of view (FOV) was $10 \times 1.50 \text{ mm}^2$ with a pixel size of $8.94 \times 3.55 \mu\text{m}^2$. The data were processed using ThorImage 5.0 and ImageJ software, taking into account the refractive index of each polymer ($n_{\text{PB72}} = 1.49$, $n_{\text{PB44}} = 1.48$, $n_{\text{Zapon}} = 1.54$) to calculate the real thickness values.

2.3. Confocal Raman Microspectroscopy (CRM)

Confocal Raman Microspectroscopy (CRM) spectra were measured in depth-profiling mode using a Renishaw inVia Raman confocal microscope equipped with a Leica DM2700 optical microscope and a 532 nm excitation source. Three depth profiles along the sample Z-axis for samples were measured by displacing the motorized microscope stage vertically relative to the laser focus with a step of 1–2 μm . The measurements were performed in an extended spectral range of 100–3200 cm^{-1} using a grating of 1800 L/mm and a thermoelectrically cooled CCD detector (spectral range 400–1060 nm) with a spectral resolution of 1 cm^{-1} per CCD pixel (functional resolution of 3 cm^{-1}). The laser power on the sample was 16 mW, with typical 10 s integration times and 1 accumulation. The data spectra were collected with a 100x long-distance objective (HC PL FLUOTAR NA = 0.75; theoretical spot size₅₃₂ = 0.43 μm , FWD = 4.7 mm) and processed with Wire5.5 and OriginPro8.5 software. The measurements were performed following the OCT profiles.

The depth-profile data were obtained by plotting the high intensity of selected bands from the polymers studied as a function of depth and calculating the full width at half-maximum (FWHM)–nominal depth (Δ)–after Gaussian fitting using OriginPro 2018 (Origin-Lab, Northampton, MA, USA) software. We calculated the corrections of nominal depths with Matlab R2021a (MathWorks, Natick, MA, USA) software.

2.4. Eddy Current (EC)

The Eddy Current (EC) measurements were performed with a portable coating thickness gauge, Leptoskop 2042 (Karl Deutsch-D), with a dual probe (Fe/NFe 0°) of 5 mm in diameter (0–3000 μm Fe, 0–1250 μm NFe). To assess the accuracy of Eddy Current analyses, we used certified calibration films provided with the device. The disks were placed over a non-magnetic and conductive substrate, and 10 measurements were recorded for each sample.

The coating thickness was estimated automatically by the instrument software; it is determined following the DIN EN ISO 2360 standard (for non-conductive layers on non-magnetic, conductive based materials). For the coating thickness range (coating < 100 μm) studied in this work, the measuring uncertainty after calibration is 1% ($\pm 1 \mu\text{m}$).

3. Results

3.1. Spectral-Domain Optical Coherence Tomography (SD-OCT)

Three profiles in the x – z axis were measured, and we later quantified the thicknesses at 12 different points for each profile. By way of example, visible images of PB72₃₀ and Zapon₂₀ polymer disks placed on graph paper and the relevant OCT B-scans are shown in Figure 2. As Figure 2b shows, the OCT data are capable of illustrating inhomogeneities and defects in the films. The polymers at higher concentrations produced typical lamella and rim dispersion after their deposition. As shown in Figure 2b, the OCT profile recorded in PB-72₃₀ samples exhibits thicker layers on the edges of the disk (rim) that become thinner in the center. OCT images also allowed for identifying defects in different areas of the film.

The samples with lower polymer concentration, e.g., Zapon₂₀ (Figure 2c,d), show thinner and more homogeneous layers. As was expected, the thickness of the layers studied is proportional to the volume of polymer dissolved in 35 μL of solution, while its homogeneity may be related to the lower viscosity of solutions with low polymer concentration and the longer time required for complete solvent evaporation.

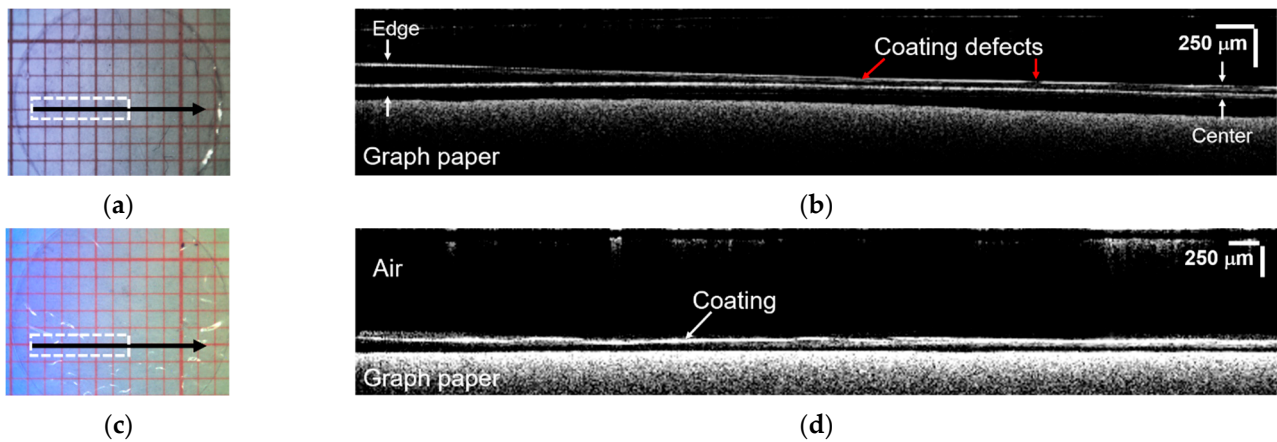


Figure 2. Visible images of (a) PB-72₃₀ and (c) Zapon₂₀ samples, the black arrows indicate the area measured with OCT and the white dashed rectangles represent the region of the profiles ($5.6 \times 1.50 \text{ mm}^2$) reported in (b,d). The red arrows highlight the coating defects found in the PB-72₃₀ sample.

Table 2 reports the results obtained with the OCT system. By plotting the thickness values as a function of sampling points (Figure 3), it is possible to observe the layer thickness distribution. Such 3D representation enables evaluation of the coating's integrity and, possibly, the quality of application over the metal surface to be conserved.

Table 2. Measured thickness results from the OCT profiles. Standard deviation is informative of thickness inhomogeneity.

Sample	Thickness Measurement (μm)												Mean (μm)	Std. dev. (μm)
	1	2	3	4	5	6	7	8	9	10	11	12		
PB-72 ₃₀	50.8	45.1	38.0	29.2	25.5	25.7	24.0	25.1	34.0	41.4	45.5	56.3	36.7	12.7
PB-72 ₂₅	34.3	32.9	29.9	25.4	23.7	21.3	20.9	19.1	20.1	31.5	45.0	36.7	28.4	9.3
PB-72 ₁₀	21.3	20.3	13.0	11.1	11.0	12.1	12.9	12.4	11.3	17.4	18.6	20.5	15.2	5.6
PB-44 ₂₅	34.3	34.8	30.7	28.4	22.0	20.5	18.5	18.9	23.7	24.8	45.8	42.4	28.7	10.0
PB-44 ₁₀	22.5	17.6	14.0	12.4	12.1	12.0	18.9	14.4	16.3	16.2	11.3	15.4	15.3	4.2
PB-44 ₅	7.3	7.0	7.4	8.4	8.4	8.3	7.4	9.6	8.4	8.3	8.4	6.9	8.0	1.4
Zapon ₇₀	7.9	8.0	6.9	7.1	6.8	7.0	9.3	6.9	7.0	6.7	7.1	7.0	18.8	5.0
Zapon ₄₀	13.7	12.9	12.9	13.0	12.8	11.6	13.1	11.6	14.1	14.9	14.0	16.5	13.4	3.4
Zapon ₂₀	7.9	8.0	6.9	7.1	6.8	7.0	9.3	6.9	7.0	6.7	7.1	7.0	7.3	1.1

3.2. Benchtop Instrumentation: Confocal Raman Microspectroscopy (CRM)

Before recording the dataset for the depth profiling analysis, the full-range spectra of each polymer were acquired (Figure 4a). Two characteristic and intense bands were selected for each polymer to evaluate thickness measurement reproducibility.

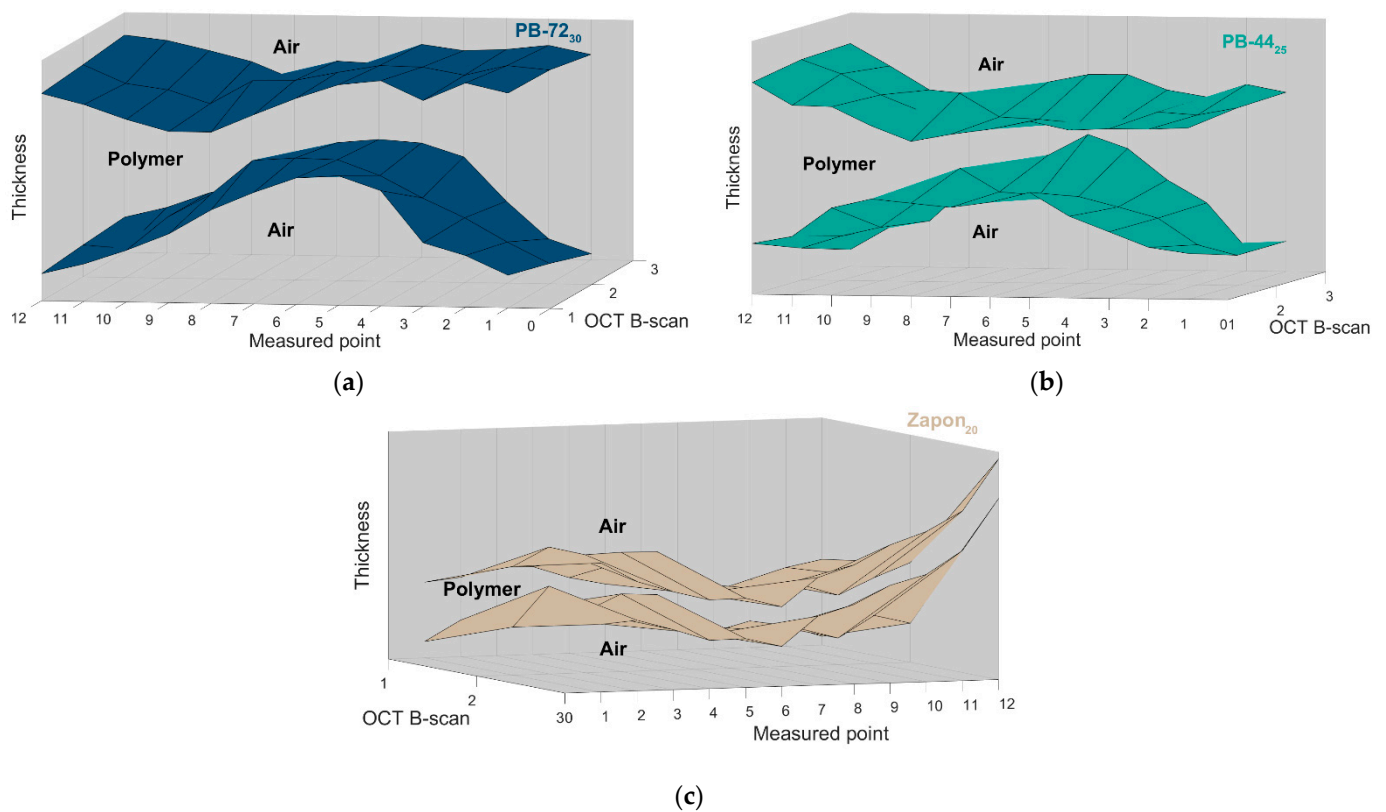


Figure 3. 3D plots of the 12 measured points extracted across three OCT B-scans for (a) PB-72₃₀, (b) PB-44₂₅, and (c) Zapon₂₀ samples showing the shape of the layers measured. The average thickness values are reported in Table 2.

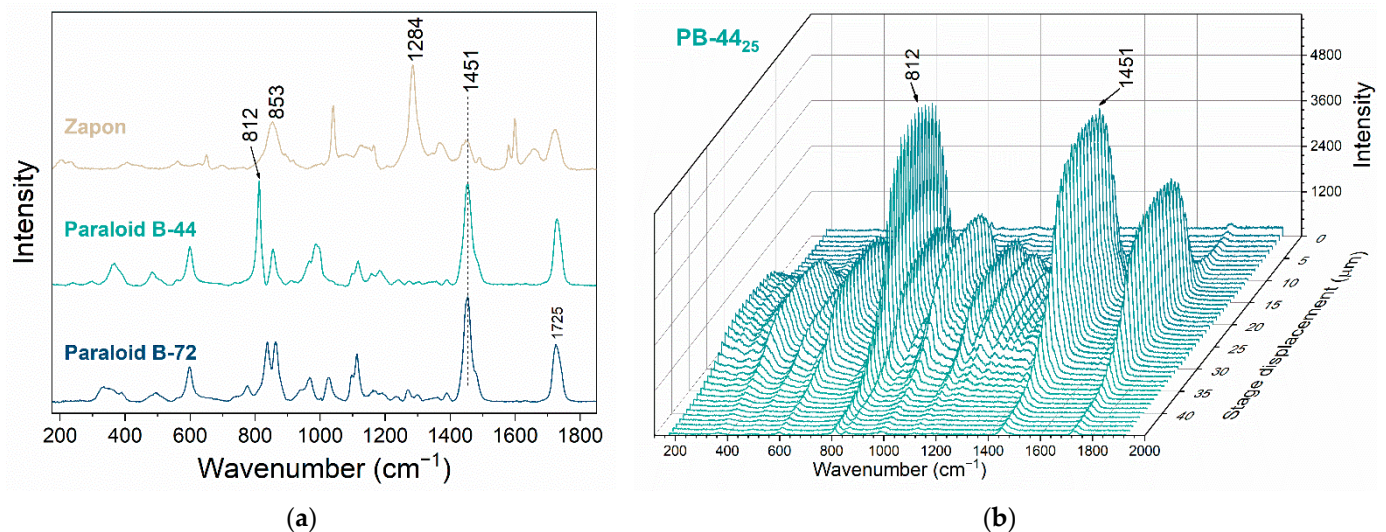


Figure 4. (a) Raman spectra from the three polymers and (b) the spectral depth profiling dataset from sample PB-44₂₅ (step of stage displacement 1 μm , 45 spectra recorded in the z axis), reported here as an example. The 812 cm^{-1} and 1451 cm^{-1} bands selected for the thickness quantification are marked with arrows.

For PB-72, the bands at 1725 cm^{-1} and 1451 cm^{-1} , assigned respectively to $\nu(\text{C}=\text{O})$ and $\delta(\text{CH}_2)$ from methylene groups, were selected. To measure PB-44 films, the bands at 1451 cm^{-1} and 812 cm^{-1} , $\delta(\text{CH}_2)$ from methylene groups and $\nu_{\text{sym}}(\text{C}-\text{C})$ from the main chain, were employed [36]. For Zapon[®] samples, thickness was calculated considering

the relative intensities of the bands at 1284 cm^{-1} and 853 cm^{-1} from $\nu_{\text{sym}}(\text{NO}_2)$ and $\nu(\text{NO})$ [37]. After setting up the experimental conditions, a sequence of spectra was recorded by focusing the laser at different depths inside the coating until the disk had been completely crossed. An example of PB-44₂₅ depth profiling is shown in Figure 4b.

The comparison between the apparent thickness data obtained with the two different selected Raman bands shows a negligible difference ($>0.6\text{ }\mu\text{m}$) (Appendix A). This confirms the possibility of choosing a distinct band in case of signal overlapping in multilayer systems (e.g., Paraloid[®] B-72 and Paraloid[®] B-44 both having an intense band at 1451 cm^{-1}). In the following discussion, we report only the results obtained with the most intense band, since they showed a lower standard deviation.

The CRM results agree with the OCT findings, showing thickness variability in the different points studied, due to the samples' inhomogeneity, and correlation between thickness and polymer concentration (Figure 5). Some differences in thickness measurement were detected due to optical aberrations produced by the refraction of the laser inside the polymeric film.

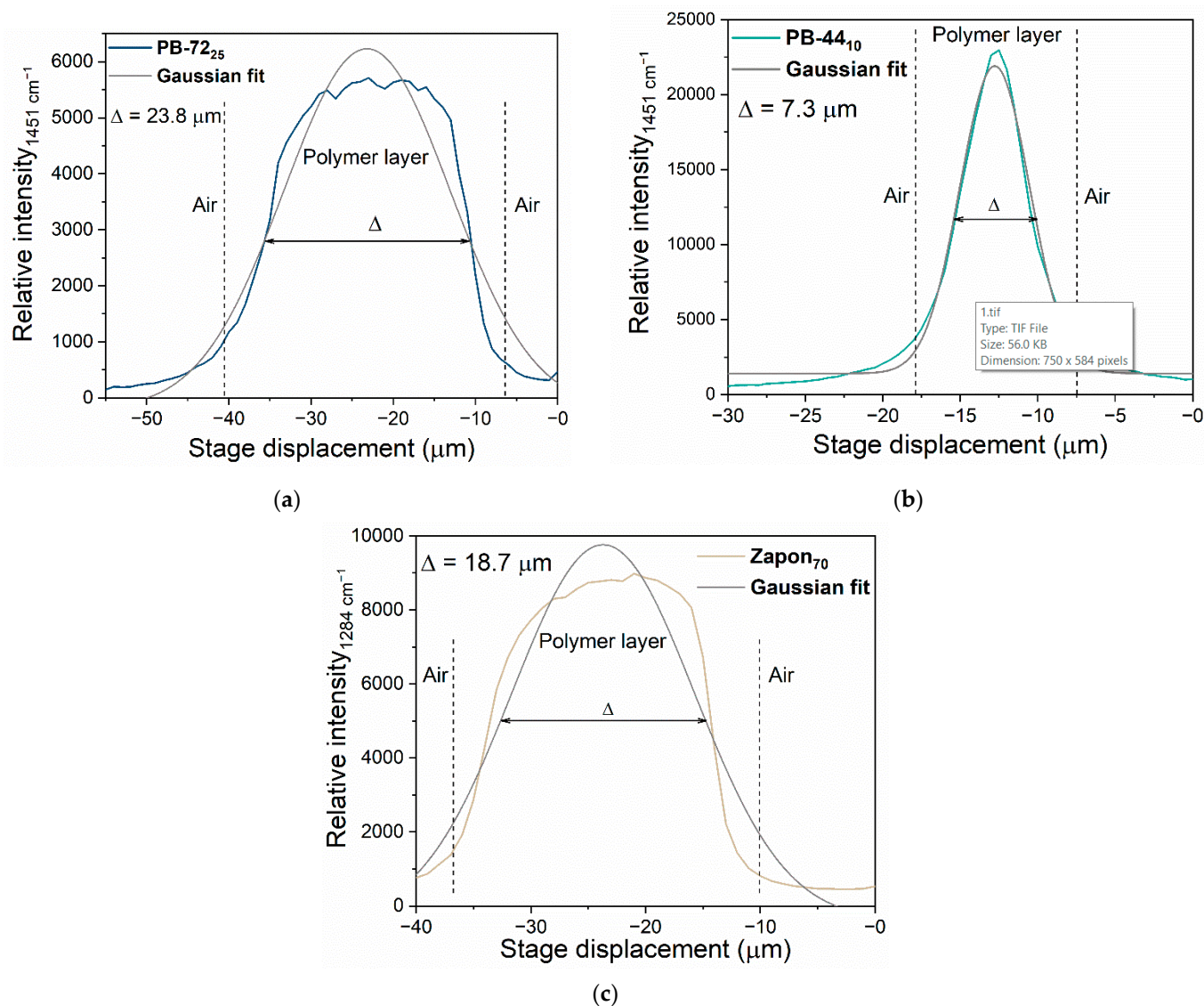


Figure 5. Relative Raman intensities registered as a function of the stage displacement of (a) PB-72 at 25% ($\delta_{\text{CH}_2} = 1451\text{ cm}^{-1}$), (b) PB-44 at 10% ($\delta_{\text{CH}_2} = 1451\text{ cm}^{-1}$), and (c) Zapon[®] at 70% ($\nu_{\text{NO}_2} = 1284\text{ cm}^{-1}$). The nominal depth (Δ)—full width at the half maximum—measured after Gaussian fit (grey line) is indicated for each sample. The values reported correspond to a single measurement.

To account for the influence of the refraction phenomenon in the thickness measurements, we calculated the corrected thickness (\bar{z}) using Equation (1) [24]:

$$\bar{z} = \frac{\int_0^1 m \cdot e^{-2m^2} \cdot (NA_{eff})^2 \cdot z(m) \cdot dm}{\int_0^1 m \cdot e^{-2m^2} \cdot (NA_{eff})^2 \cdot dm}; \tag{1}$$

the equation considers the true point of focus of the laser ($z(m)$) and the weighting factor ($(NA_{eff})^2$) that accounts for the volume from which emitted photons can be captured by the objective [38]. As proposed by Everall [39], $z(m)$ can be calculated as:

$$z(m) = \Delta \left[m^2 \cdot \frac{NA^2(n^2 - 1)}{(1 - NA^2)} + n^2 \right]^{0.5}, \tag{2}$$

where Δ is the nominal depth (thickness) as obtained from the FWHM measurement from the profile, NA the objective numerical aperture, n the polymer refractive index, and m the normalized radius. On the other hand, $(NA_{eff})^2$ is obtained with Equation (3):

$$(NA_{eff})^2 = \frac{1}{n^2} \left[\frac{m^2 \cdot NA^2}{1 - NA^2 + m^2 \cdot NA^2} \right], \tag{3}$$

Table 3 summarizes the nominal depth (Δ) measured for each sample and the corrected thickness (\bar{z}). As expected, laser refraction has a higher influence when studying thicker layers producing a higher error value (h_z), as calculated with Equation (4) [24].

$$h_z = 1.34 \left[\frac{\int_0^1 m \cdot e^{-2m^2} \cdot (NA_{eff})^2 \cdot z^2(m) \cdot dm}{\int_0^1 m \cdot e^{-2m^2} \cdot (NA_{eff})^2 \cdot dm} - \bar{z}^2 \right]^{0.5}, \tag{4}$$

Table 3. Average CRM results from three measures: nominal depth (Δ) as measured by the instrument compared to the corrected thickness (\bar{z}), with the higher error value (h_z).

Sample	Δ (μm)	Std. dev. (μm)	\bar{z} (μm)	Std. dev. (μm)	h_z
PB-72 ₃₀	41.8	3.2	62.3	4.8	10.6
PB-72 ₂₅	24.2	0.5	36.1	0.8	8.0
PB-72 ₁₀	5.5	1.0	8.3	0.0	3.8
PB-44 ₂₅	18.7	1.2	27.7	1.7	7.0
PB-44 ₁₀	8.3	1.5	12.3	2.3	4.7
PB-44 ₅	5.6	0.8	8.2	1.1	3.8
Zapon ₇₀	18.2	0.5	28.1	0.8	7.1
Zapon ₄₀	6.7	0.6	9.5	0.6	4.1
Zapon ₂₀	3.5	0.3	5.5	0.3	3.1

Yet, CRM provides a good estimate of the thickness of the protective layers, being sensible even to slight variations. Additionally, CRM is capable of obtaining chemical information relevant for the assessment of degradation processes, possible mixtures (e.g., pigmented coatings), or inclusions in the layer [20].

4. Discussion: Optical vs. Electromagnetic Methods

Table 4 summarizes the results obtained with the three techniques. Besides the mean thickness values, for OCT and CRM the minimum and maximum thicknesses are reported to indicate their variability. In the first place, it is necessary to consider the different sizes of the areas analyzed. The EC system employed in this work offers average information from an area of 19.63 mm² (\varnothing 5 mm), while the optical methods provide information with a microscopic resolution, thus registering variability throughout the film.

Table 4. Comparison of thickness measurements obtained with the three techniques: OCT, CRM, and EC.

Sample	OCT (μm) Min./Max.	OCT Mean (μm)	Std. dev. (μm)	CRM \bar{z} (μm) Min./Max.	CRM \bar{z} Mean (μm)	Std. dev. (μm)	Eddy Current $\varnothing 5 \text{ mm}$ (μm)	Std. dev. (μm)
PB-72 ₃₀	21.3/60.3	36.7	12.7	57.9/67.4	62.3	4.8	43	2
PB-72 ₂₅	17.7/50.1	28.4	9.3	23.8/36.6	36.1	0.8	32	2
PB-72 ₁₀	8.9/32.8	15.2	5.6	6.7/9.7	8.2	1.5	12	1
PB-44 ₂₅	17.7/50.0	28.7	10.0	25.8/29.2	27.7	1.7	30	1
PB-44 ₁₀	7.7/25.3	15.3	4.2	10.8/14.9	12.3	2.3	10	1
PB-44 ₅	6.6/11.1	8.0	1.4	7.2/9.5	8.2	1.1	6	1
Zapon ₇₀	9.8/28.4	18.8	5.0	27.5/29.0	28.1	0.8	20	1
Zapon ₄₀	7.4/21.2	13.4	3.4	9.0/10.2	9.5	0.6	10	1
Zapon ₂₀	6.5/10.6	7.3	1.1	5.1/5.8	5.5	0.3	4	1

Despite the variability of the thickness values measured with the three techniques, the results are comparable. It is worth noticing that, in addition to the mean values, OCT and CRM data show the minimum and maximum thickness of the layers at a microscopic scale. Spot CRM results depend on the area analyzed; however, performing a depth-profile mapping could solve this issue, offering a profile comparable to the OCT results.

The results from the thinner samples (i.e., the ones obtained with lower polymer concentration solutions) showed lower variability for the three techniques due to the homogeneity of the layers. This points to the main disadvantage of the EC: irregularities in the coating are not registered due to the averaging area. Moreover, OCT and CRM offer morphological information about the layer, thus registering the topography of the coating induced by possible irregularities present in the metallic surface; this feature is not registered by EC.

Regarding the presence of corrosion products in the metallic surface, such as passive patina layers, the optical methods are not affected by them. OCT registers changes in the refractive index and, consequently, the corrosion patina does not interfere in the estimation of the polymeric layers. Accordingly, CRM is able to differentiate between the polymeric coatings and the metallic patina/surface. The main advantage of CRM is the possibility to simultaneously characterize the corrosion products present and, in some cases, the possible inclusions (i.e., colorants in artificial patinas) in the coating layers [20]. On the contrary, EC results may be influenced by the presence of corrosion products under the coating layer and even by superficial deposits (i.e., dust). It either includes their thickness in the estimation of the polymeric coating or potentially detects a multilayer system without a specific identification, since it exclusively registers conductivity differences.

In contrast, CRM, as used in this study, is non-portable and only samples that can fit under the microscope can be studied. Additionally, fluorescence emission by the probed material can interfere with the profile measurements. Ultimately, the measurements are highly time consuming. Both OCT and CRM require corrections for the material refraction index.

Table 5 summarizes the main features of each technique. The choice of one or the other must be evaluated according to the object's characteristics. The optical methods offer more detailed results by registering micrometric coating features; however, ready-to-use (i.e., not requiring mathematical corrections), fast, and in situ measurements can be performed with ECs.

Table 5. Main features of each technique employed in this work.

Technique	Portable	Area Investigated ¹	Data Correction	Contactless	Measure Time	Corrosion Interference
OCT	Yes	Smallest area: 13 μm^2	Yes	Yes	Relatively fast	No
CRM	No	Smallest area: $\sim 1.77 \mu\text{m}^2$ ($\varnothing 1.5 \mu\text{m}$)	Yes	Yes	Slow	No
EC	Yes	19.63 mm^2 ($\varnothing 5 \text{ mm}$)	No	No	Fast	Yes

¹ For the systems tested in this work.

5. Conclusions

Protective coatings have a significant role in metallic cultural heritage preservation. The evaluation of layer features, such as thickness estimation, fractures or interstice identification, and the detection of chemical changes, contributes to the monitoring of their performance. The three techniques tested in this work are not interchangeable and each one showed specific advantages and disadvantages, such as the possibility to identify detailed layer features or the identification of chemical composition. The results of the two optical techniques (OCT and CRM) are in reasonable agreement and revealed the layers' inhomogeneity; their image and graphical outputs are easy and fast to interpret but require corrections considering the refractive index of the polymer. In contrast, CRM, as used in this study, is not portable and the object's size and shape may therefore limit its employment. However, the recent advances in portable Raman instrumentation may allow the in situ analysis of coatings using the confocal modality.

The EC measurements agree with the other two techniques when homogeneous layers are tested; however, the main issue with ECs is that the results are averaged over a relatively big area, thus hampering the detectability of microscale inhomogeneities and defects in the polymer coatings. Additionally, corrosion products and deposits over the surface can interfere with thickness estimation.

All in all, compared to electrochemical methods, the optical techniques allow for more features from the polymeric layers to be registered yet require specialized instrumentation. In the future, this issue might be solved by more user-friendly systems being made available to conservators.

Author Contributions: Conceptualization, R.F. and J.S.; methodology, A.D.F., R.F. and J.S.; formal analysis, D.Q.B., A.D.F., D.P., A.C., S.P., R.F. and J.S.; investigation, D.Q.B. and D.P.; data curation, D.Q.B., R.F. and J.S.; writing—original draft preparation, D.Q.B. and J.S.; writing—review and editing, D.Q.B., A.D.F., D.P., A.C., S.P., R.F. and J.S.; supervision, R.F. and J.S.; project administration, R.F. and J.S.; funding acquisition, R.F. and J.S. All authors have read and agreed to the published version of the manuscript.

Funding: This research was funded by Regione Toscana (POR FSE 2014–2020, “Giovani”, Intervention Program “CNR4C”, RS4Art and SuperTech3D projects, CUP B15J19001040004).

Institutional Review Board Statement: Not applicable.

Informed Consent Statement: Not applicable.

Data Availability Statement: The data presented in this study are available on reasonable request from the corresponding author.

Conflicts of Interest: The authors declare no conflict of interest.

Appendix A

Sample	Band (cm ⁻¹)	Δ (μm)	Std. dev. (μm)	Difference (μm)
PB-72 ₃₀	1725	42.32	3.44	0.54
	1451	41.78	3.22	
PB-44 ₂₅	1451	18.69	1.16	0.05
	812	18.64	1.23	
Zapon ₇₀	1284	18.17	0.49	0.19
	854	17.98	0.68	

References

1. Fayomi, O.S.I.; Akande, I.G.; Odigie, S. Economic Impact of Corrosion in Oil Sectors and Prevention: An Overview. *J. Phys. Conf. Ser.* **2019**, *1378*, 022037. [[CrossRef](#)]
2. Cano, E.; Lafuente, D.; Bastidas, D.M. Use of EIS for the evaluation of the protective properties of coatings for metallic cultural heritage: A review. *J. Solid State Electrochem.* **2010**, *14*, 381–391. [[CrossRef](#)]
3. Scott, D.A. *Copper and Bronze in Art. Corrosion, Colorants, Conservation*; The Getty Conservation Institute: Los Angeles, CA, USA, 2002; ISBN 0-89236-638-9.
4. Cano, E.; Bastidas, D.M.; Argyropoulos, V.; Fajardo, S.; Siatou, A.; Bastidas, J.M.; Degryny, C. Electrochemical characterization of organic coatings for protection of historic steel artefacts. *J. Solid State Electrochem.* **2010**, *14*, 453–463. [[CrossRef](#)]
5. Kovács, R.L.; Daróczy, L.; Barkóczy, P.; Baradács, E.; Bakonyi, E.; Kovács, S.; Erdélyi, Z. Water vapor transmission properties of acrylic organic coatings. *J. Coat. Technol. Res.* **2021**, *18*, 523–534. [[CrossRef](#)]
6. Favaro, M.; Mendichi, R.; Ossola, F.; Russo, U.; Simon, S.; Tomasin, P.; Vigato, P.A. Evaluation of polymers for conservation treatments of outdoor exposed stone monuments. Part I: Photo-oxidative weathering. *Polym. Degrad. Stab.* **2006**, *91*, 3083–3096. [[CrossRef](#)]
7. Artesani, A.; Di Turo, F.; Zucchelli, M.; Traviglia, A. Recent Advances in Protective Coatings for Cultural Heritage—An Overview. *Coatings* **2020**, *10*, 217. [[CrossRef](#)]
8. Letardi, P. Testing New Coatings for Outdoor Bronze Monuments: A Methodological Overview. *Coatings* **2021**, *11*, 131. [[CrossRef](#)]
9. England, A.; Hosbein, K.; Price, C.; Wylder, M.; Miller, K.; Clare, T. Assessing the Protective Quality of Wax Coatings on Bronze Sculptures Using Hydrogel Patches in Impedance Measurements. *Coatings* **2016**, *6*, 45. [[CrossRef](#)]
10. Agnoletti, S.; Bruni, T.; Cagnini, A.; Galeotti, M.; Porcinai, S. Le applicazioni della tecnica delle correnti indotte (Eddy-Current) per la conservazione e lo studio di manufatti metallici di valore storico-artistico. *OPD Restauro* **2016**, *28*, 162–173.
11. Sousa, J.B.; Ventura, J.O.; Pereira, A. Noncontact techniques. In *Transport Phenomena in Micro- and Nanoscale Functional Materials and Devices*; Elsevier: Amsterdam, The Netherlands, 2021; pp. 273–307. ISBN 978-0-323-46097-2.
12. García-Martín, J.; Gómez-Gil, J.; Vázquez-Sánchez, E. Non-Destructive Techniques Based on Eddy Current Testing. *Sensors* **2011**, *11*, 2525–2565. [[CrossRef](#)] [[PubMed](#)]
13. Meng, X.; Lu, M.; Yin, W.; Bennecer, A.; Kirk, K.J. Evaluation of Coating Thickness Using Lift-Off Insensitivity of Eddy Current Sensor. *Sensors* **2021**, *21*, 419. [[CrossRef](#)] [[PubMed](#)]
14. Lenz, M.; Mazzon, C.; Dillmann, C.; Gerhardt, N.; Welp, H.; Prange, M.; Hofmann, M. Spectral Domain Optical Coherence Tomography for Non-Destructive Testing of Protection Coatings on Metal Substrates. *Appl. Sci.* **2017**, *7*, 364. [[CrossRef](#)]
15. Porcinai, S.; Ferretti, M. X-ray fluorescence-based methods to measure the thickness of protective organic coatings on ancient silver artefacts. *Spectrochim. Acta Part B At. Spectrosc.* **2018**, *149*, 184–189. [[CrossRef](#)]
16. Porcinai, S.; Heginbotham, A. Thickness mapping of organic layers applied on sterling silver by means of X-ray fluorescence scanning. *Spectrochim. Acta Part B At. Spectrosc.* **2021**, *180*, 106158. [[CrossRef](#)]
17. Catelli, E.; Sciutto, G.; Prati, S.; Jia, Y.; Mazzeo, R. Characterization of outdoor bronze monument patinas: The potentialities of near-infrared spectroscopic analysis. *Environ. Sci. Pollut. Res.* **2018**, *25*, 24379–24393. [[CrossRef](#)] [[PubMed](#)]
18. Crawford, M.K.; Fair, L.; Rovito, K.; Polidori, T.; Grayburn, R. Thickness Measurements of Clear Coatings on Silver Objects using Fiber Optic Reflectance Spectroscopy. *J. Am. Inst. Conserv.* **2021**, *61*, 71–84. [[CrossRef](#)]
19. Barra, V.; Daffara, C.; Porcinai, S.; Galeotti, M. Application of coatings on silver studied with punctual and imaging techniques: From specimens to real cases. *IOP Conf. Ser. Mater. Sci. Eng.* **2018**, *364*, 012059. [[CrossRef](#)]
20. Dal Fovo, A.; Mattana, S.; Chaban, A.; Quintero Balbas, D.; Lagarto, J.L.; Striova, J.; Cicchi, R.; Fontana, R. Fluorescence Lifetime Phasor Analysis and Raman Spectroscopy of Pigmented Organic Binders and Coatings Used in Artworks. *Appl. Sci.* **2021**, *12*, 179. [[CrossRef](#)]
21. Boyatzis, S.C.; Douvas, A.M.; Argyropoulos, V.; Siatou, A.; Vlachopoulou, M. Characterization of a Water-Dispersible Metal Protective Coating with Fourier Transform Infrared Spectroscopy, Modulated Differential Scanning Calorimetry, and Ellipsometry. *Appl. Spectrosc.* **2012**, *66*, 580–590. [[CrossRef](#)]
22. Antoniuk, P.; Strąkowski, M.R.; Pluciński, J.; Kosmowski, B.B. Non-destructive inspection of anti-corrosion protective coatings using Optical Coherent Tomography. *Metrol. Meas. Syst.* **2012**, *XIX*, 365–372. [[CrossRef](#)]
23. Tomba, J.P.; de la Paz Miguel, M.; Perez, C.J. Correction of optical distortions in dry depth profiling with confocal Raman microspectroscopy: Distortion correction in dry depth profiling with confocal Raman microspectroscopy. *J. Raman Spectrosc.* **2011**, *42*, 1330–1334. [[CrossRef](#)]
24. Lorenzetti, G.; Striova, J.; Zoppi, A.; Castellucci, E.M. Confocal Raman microscopy for in depth analysis in the field of cultural heritage. *J. Mol. Struct.* **2011**, *993*, 97–103. [[CrossRef](#)]
25. Everall, N.J. Confocal Raman microscopy: Common errors and artefacts. *Analyst* **2010**, *135*, 2512–2522. [[CrossRef](#)] [[PubMed](#)]
26. Schmidt, U.; Ibach, W.; Mueller, J.; Hollricher, O. The Confocal Raman AFM: A Powerful Tool for the Characterization of Surface Coatings. In *Optical Measurement Systems for Industrial Inspection V*; Osten, W., Gorecki, C., Novak, E.L., Eds.; Proc. SPIE: Munich, Germany, 2007; Volume 66160E, pp. 119–124. [[CrossRef](#)]
27. Ntelia, E.; Karapanagiotis, I. Superhydrophobic Paraloid B72. *Prog. Org. Coat.* **2020**, *139*, 105224. [[CrossRef](#)]
28. Tennent, N.H.; Townsend, J.H. The significance of the refractive index of adhesives for glass repair. *Stud. Conserv.* **1984**, *29*, 205–212. [[CrossRef](#)]

29. Down, J.L.; MacDonald, M.A.; Tétreault, J.; Williams, A.S. Adhesive Testing at the Canadian Conservation Institute: An Evaluation of Selected Poly(Vinyl Acetate) and Acrylic Adhesives. *Stud. Conserv.* **1996**, *41*, 19–44.
30. Vinçotte, A.; Beauvoit, E.; Boyard, N.; Guilminot, E. Effect of solvent on PARALOID[®] B72 and B44 acrylic resins used as adhesives in conservation. *Herit. Sci.* **2019**, *7*, 42. [[CrossRef](#)]
31. Argyropoulos, V.; Giannoulaki, M.; Michalakakos, G.P.; Siatou, A. *A Survey of the Types of Corrosion Inhibitors and Protective Coatings Used for the Conservation of Metal Objects from Museum Collections in the Mediterranean Basin*; Department of Conservation of Antiquities and Works of Art & T.E.I. of Athens: Cairo, Egypt, 2007; pp. 1–5.
32. Holben Ellis, M. The Shifting Function of Artists' Fixatives. *J. Am. Inst. Conserv.* **1996**, *35*, 239–254. [[CrossRef](#)]
33. Conn, G.K.T.; Eaton, G.K. On Polarization by Transmission with Particular Reference to Selenium Films in the Infrared. *J. Opt. Soc. Am.* **1954**, *44*, 553–557. [[CrossRef](#)]
34. Chapman, S.; Mason, D. Literature Review: The use of Paraloid B-72 as a surface consolidant for stained glass. *J. Am. Inst. Conserv.* **2003**, *42*, 381–392. [[CrossRef](#)]
35. Paraloid B-44—CAMEO. Available online: https://cameo.mfa.org/wiki/Paraloid_B-44 (accessed on 14 June 2022).
36. Ohlidalová, M.; Kučerová, I.; Novotná, M. Identification of acrylic consolidants in wood by Raman spectroscopy. *J. Raman Spectrosc.* **2006**, *37*, 1179–1185. [[CrossRef](#)]
37. Neves, A.; Angelin, E.M.; Roldão, É.; Melo, M.J. New insights into the degradation mechanism of cellulose nitrate in cinematographic films by Raman microscopy. *J. Raman Spectrosc.* **2019**, *50*, 202–212. [[CrossRef](#)]
38. Tfayli, A.; Piot, O.; Manfait, M. Confocal Raman microspectroscopy on excised human skin: Uncertainties in depth profiling and mathematical correction applied to dermatological drug permeation. *J. Biophotonics* **2008**, *1*, 140–153. [[CrossRef](#)] [[PubMed](#)]
39. Everall, N.J. Confocal Raman Microscopy: Why the Depth Resolution and Spatial Accuracy Can Be Much Worse Than You Think. *Appl. Spectrosc.* **2000**, *54*, 1515–1520. [[CrossRef](#)]